Slip Flow through Colloidal Crystals of Varying Particle Diameter

Benjamin J. Rogers and Mary J. Wirth*

Department of Chemistry, Purdue University, 560 Oval Drive, West Lafayette, Indiana 47907, United States

ABSTRACT Slip flow of water through silica colloidal crystals was investigated experimentally for eight different particle diameters, which have hydraulic channel radii ranging from 15 to 800 nm. The particle surfaces were silylated to be low in energy, with a water contact angle of 83°, as determined for a silylated flat surface. Flow rates through centimeter lengths of colloidal crystal were measured using a commercial liquid chromatograph for accurate comparisons of water and toluene flow rates using pressure gradients as high as 10^{10} Pa/m. Toluene exhibited no-slip Hagen–Poiseuille flow for all hydraulic channel radii. For water, the slip flow enhancement as a function of hydraulic channel radius was described well by the expected slip flow correction for Hagen–Poiseuille flow, and the data revealed a constant slip length of 63 ± 3 nm. A flow enhancement of 20 ± 2 was observed for the smallest hydraulic channel radius of 15 nm. The amount of slip flow was found to be independent of shear rate over a range of fluid velocities from 0.7 to 5.8 mm/s. The results support the applicability of the slip flow correction for channel radii as small as 15 nm. The work demonstrates that packed beds of submicrometer particles enable slip flow to be employed for high-volume flow rates.

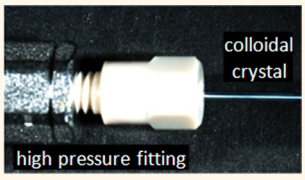

KEYWORDS: slip flow · silica colloidal crystal · flow enhancement

Slip flow is an important phenomenon in nanofluidics, whereby flow enhancement is caused by weak interactions between the fluid and the wall. The interest in slip flow has intensified after reports of $>10^3$ flow enhancements of water in carbon nanotubes.[1,2] Potential applications of such unexpectedly high flow rates for water are lower energy costs in the desalination of seawater[3,4] and high efficiency chromatography of pharmaceuticals produced through biotechnology.[5] The flattening of the parabolic flow profile by slip flow promises an especially large impact on chromatography because the flow profile is the fundamental limitation to the reduction of zone broadening.[6]

Slip flow is described by an enhancement in flow rate, E, which is the ratio of the flow rate with slip, Q_{slip}, to the flow rate expected in the limit of no slip, $Q_{no\text{-}slip}$.[7] The amount of flow enhancement for a cylinder of radius r is determined by the slip length, L_s, as described by eq 1:

$$E = \frac{Q_{slip}}{Q_{no\text{-}slip}} = 1 + \frac{4L_s}{r} \qquad (1)$$

The aforementioned carbon nanotube results disagree with one another with regard to the role of the channel radius of eq 1: the wider multiwalled nanotube, 7 nm i.d.,[2] gave an order of magnitude higher flow enhancement than did the double-walled nanotube of ≤2 nm i.d.[1] The larger carbon nanotubes exhibited slip lengths on the micrometer scale. Molecular dynamics simulations indicate that carbon nanotubes of diameters above 5 nm should exhibit a slip length on the order of 30 nm, and below 5 nm the effect of the depletion layer at the surface becomes significant, reducing the average viscosity and greatly increasing slip length.[8,9] Experimental measurements of slip lengths for water through other types of carbonaceous channels of wider diameter are almost all well below 1 μm for larger channel radii, and slip lengths are not consistent with one another. For example, negligible slip was observed for graphitic nanopipes of 300 nm i.d,[10] but slip was observed for nanopipes of amorphous carbon of 44 nm i.d., with a slip length of 35 ± 3 nm for water and 41 ± 2 for decane.[11] For channel diameters greater than 1 μm, many measurements of slip lengths have been made, with wide disagreement. For example, slip lengths were in agreement to be 30 nm for two different flow studies of microscale channels[12,13] and also for a micrometer diameter capillary.[14] Slip lengths were 50 nm in one case[15] and 1 μm in another case,[16] each from velocimetry measurements of flow in microchannels.

* Address correspondence to mwirth@purdue.edu.

Received for review October 29, 2012 and accepted December 13, 2012.

Published online December 13, 2012
10.1021/nn305028f

The slip length was too noisy to report for another velocimetry experiment, except to show that it is not detectably longer than 100 nm.[17] A longer slip length, 175 ± 50 nm, was measured by fluorescence recovery after photobleaching of a tracer dye in the evanescent field for hexadecane flowing past sapphire.[18] The hexadecane/sapphire system is also low wetting, as its interfacial energy would be similar to that of water/hydrocarbon interfaces. The experimental results are in remarkable disagreement.

Molecular dynamics simulations point out an additional factor contributing to the slip length, which is contact angle.[19] Presumably, slip length would reach zero in the limit of zero contact angle in the continuum limit. Contact angles are largely unreported in the experimental studies. The contact angle has been related to the interaction energy between water and the nanotube surface,[20] and this has been used to derive a relation to account for contact angle in slip flow.[21] A review of flow in carbon nanotubes shows from TEM images of water trapped in closed carbon nanotubes that contact angles vary over 90°.[22] Since contact angles were not measured for the same nanotubes that were used for slip flow measurements, it is difficult to retrospectively explain slip lengths. While oxidation is obviously a factor increasing hydrophilicity, the wall thickness of the nanotube might also be a factor affecting contact angle: experiments show that a single monolayer of graphene is transparent with respect to wetting, and at least six layers of graphene to shield the water from the substance on the other side of graphene.[23] The lack of knowledge of these important parameters is likely a main reason for the disagreement, and the difficulty of measuring flow through nanopores without artifacts is possibly a contributing reason.

Experimental study is needed for channels that are more thoroughly characterized: the channel radius is on the order of the slip length to obtain sufficient slip flow, the length of the medium is sufficiently long that spurious electric fields cannot contribute to flow, the surfaces have known, high contact angle, there is assurance that gas bubbles are absent, and there are control measurements with a wetting liquid for the same channels. The purpose of this work is to implement these controls to test the applicability of eq 1 for nanoscale pores. This is possible by using silica colloidal crystals, which have been shown to pack uniformly into capillaries, to give nanoscale channel dimensions, to be chemically modified to have a high contact angle for water, to allow pressures exceeding 1 GPa/m, and to give significant slip flow.[5] The surface is chemically modified through mixed self-assembly of butyl and methyl trichlorosilanes.[24] The system used in this work is summarized in Figure 1, which shows (A) a packed capillary in a high-pressure flow connector for a 2 cm long length of colloidal crystal, (B) a droplet of water on a flat fused silica surface treated with the same silane to show the contact angle of 83°, and (C) an SEM image showing high crystallinity of the packing to give nanoscale channels. While a surface with a contact angle of 83° for water is often referred to as hydrophobic, we refer to this as a low-energy surface or a low-wetting surface for water. This is consistent with the terminology of de Gennes *et al.*, who use hydrophobic and hydrophilic for contact angles above and below 90°, respectively, for water.[25] In this work the particle size is varied, allowing many different channel radii to be studied.

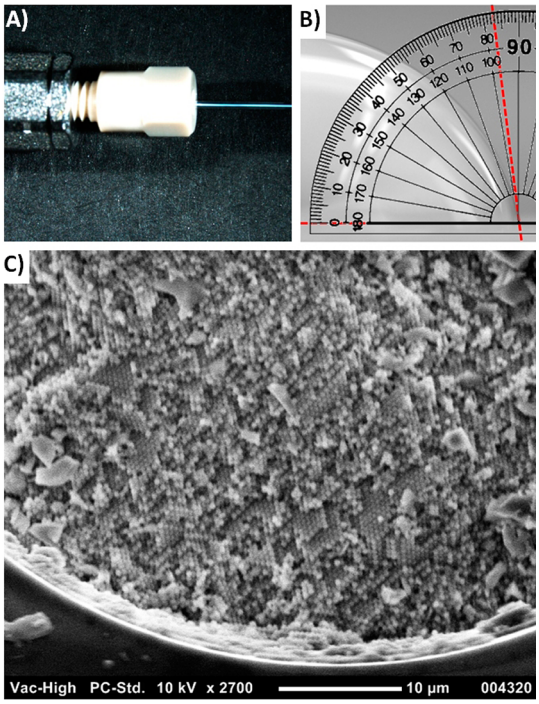

Figure 1. Summary of the type of system studied in this work. (A) High-pressure fittings are used to measure flow through capillaries packed with colloidal silica. The blue color is visible from the Bragg diffraction of 470 nm particles in this example. (B) The surface of the colloidal silica has a monolayer of hydrophobic silane, which is shown to give a contact angle of 83° on a flat fused silica slide bearing the same silane. (C) An SEM image of a capillary packed with 470 nm particles, in this example showing significant face-centered-cubic crystalline order.

For packed spheres, the effective channel radius is described by the hydraulic radius, which is the radius of the equivalent cylinder with the same flow resistance. The hydraulic radius, r_{hyd}, is calculated from the particle diameter, d_p, using ε as the liquid volume fraction of the medium.[26]

$$r_{hyd} = \frac{d_p}{3}\frac{\varepsilon}{(1-\varepsilon)} \quad (2)$$

The hydraulic radius is used in eq 1 to calculate slip length from the observed flow rate. The value of ε is determined independently from flow measurements by using the ratio of the hindered diffusion coefficient, D^*, to the diffusion coefficient in open solution, D,

measured by fluorescence recovery after photobleaching (FRAP).

$$D^* = \varepsilon D \quad (3)$$

Equation 3 arises from the proportionality between electrophoretic mobility and the free volume fraction and, in turn, the proportionality between electrophoretic mobility and the diffusion coefficient through their common friction coefficient.[27,28]

In the no-slip limit, the Kozeny–Carman equation has been shown to describe Hagen–Poiseuille flow through packed spheres very well.[29] The Kozeny–Carman equation describes the empty tower velocity, v, which is the velocity outside of the packed bed, as a function of pressure, P, and bed length, L, in the limit of no slip.

$$\frac{P}{L} = \frac{180v\eta}{{d_p}^2}\frac{(1-\varepsilon)^2}{\varepsilon^3} \quad (4)$$

In this equation η is the fluid viscosity and d_p is the particle diameter. The volume flow rate, Q, is simply the empty tower velocity times the cross-sectional area of the capillary, with its radius, R.

$$Q = v\pi R^2 \quad (5)$$

In this work, the predicted value for Q, from independently determining all other variables of eqs 4 and 5, is compared to the experimentally measured value of Q for wetting and nonwetting liquids to characterize flow enhancement for a series of channel radii ranging from 15 to 800 nm.

RESULTS AND DISCUSSION

Table 1 lists the value of porosity, ε, for each particle diameter, as determined by the ratio of the diffusion coefficient for fluorescein inside and outside of the colloidal crystal under nonadsorbing conditions. These porosities increase from $\varepsilon = 0.26$, for the smallest particles, which approaches perfect face-centered-cubic crystallinity ($\varepsilon = 0.256$), to nearly $\varepsilon = 0.40$ for the largest particles, which represents random packing.

The volume flow rates, Q, for two fluids, water and toluene, are compared, representing a poorly wetting liquid ($\theta_{contact} = 83°$) and a wetting liquid ($\theta_{contact} = 0°$), respectively. The bulk viscosities of the two liquids at 25 °C were adjusted for pressure using the data of Thompson *et al.* for water[30] and Dymond *et al.* for toluene.[31] The water was thermostated by the chromatograph to maintain constant temperature. The toluene was not thermostated, but its temperature dependence is weak, ~1% per °C at room temperature. Figure 2 shows flow rate data for three different particle sizes, and the remainder of the flow rate data are detailed in the Supporting Information. The flow rates are normalized for viscosity, which allows water and toluene to be compared, and also normalized for column length, since each capillary had a slightly different length. All lengths were on the order of 2 cm. Figure 2a presents the data for the largest particle diameter, 3.6 μm, showing that the slopes for water and toluene are indistinguishable. The flow enhancement is 1.02 ± 0.02, where the high precision is due to the use of a commercial HPLC instrument, which is designed for use with particle diameters on the order of a few micrometers. Since the hydraulic radius is 800 nm, negligible slip flow is expected. Figure 2b shows flow rate data for an intermediate sized particle, 1.3 μm, which has a hydraulic radius of 210 nm. A significant amount of slip flow is now evident, with water having twice the normalized flow rate of toluene. The dashed line is the calculated line from the Kozeny–Carman relation using eqs 4 and 5, and it virtually overlaps the toluene data. This indicates that toluene has negligible slip flow. The ratio of slopes for water and toluene shows that the flow enhancement is 2.4 ± 0.2, where the error is the standard deviation calculated from the propagated errors of the slopes from the linear regressions of the flow rate data for the two liquids. Figure 2c presents the normalized flow rate data for the smallest particles, which are 125 nm in diameter, with a hydraulic radius of 15 nm. The slopes are now drastically different for water and toluene. Figure 2d shows the toluene data for the 125 nm particles on an expanded scale, along with the line predicted from the parameters that go into the Kozeny–Carman equation. The toluene data follow the Kozeny–Carman line within experimental error. This indicates that toluene has negligible slip flow even for the hydraulic radius of 15 nm. Since the viscosity of toluene is about half that of water, the actual flow rate of water is about 10 times that of toluene. From the ratio of slopes, the flow enhancement is 20 ± 2 for a 15 nm hydraulic radius.

The plots of pressure *vs* flow rate for the remaining particles are provided in the Supporting Information. These data are summarized in Table 1, along with the flow rate data of Figure 2. The errors in the flow rates

TABLE 1. Summary of Measured Parameters for Each Particle Diameter, d_p: Porosity (ε), Hydraulic Radius, r_{hyd}, the Calculated Slope for No-Slip Hagen–Poiseuille Flow (m(HP)), and Measured Slopes for Flow Rate *vs* Pressure for Toluene and Water (m(toluene)) and m(water))[a]

d_p	ε	r_{hyd}	m(HP)	m(toluene)	m(water)	E
125	0.26	15	0.0068	0.0068 ± 0.0004	0.14 ± 0.01	20 ± 2
220	0.26	26	0.022	0.024 ± 0.002	0.27 ± 0.007	11 ± 1
330	0.27	41	0.06	0.061 ± 0.004	0.41 ± 0.01	6.7 ± 0.5
470	0.28	59	0.128	0.13 ± 0.01	0.67 ± 0.03	5.1 ± 0.5
660	0.29	90	0.31	0.33 ± 0.02	1.33 ± 0.2	4.0 ± 0.7
880	0.3	126	0.628	0.67 ± 0.02	2.4 ± 0.2	3.6 ± 0.3
1300	0.33	213	1.992	2.01 ± 0.09	4.15 ± 0.07	2.1 ± 0.1
3600	0.4	800		34.8 ± 0.6	35.6 ± 0.2	1.02 ± 0.02

[a] All lengths are in units of nm. The slopes are in units of nL · cP · cm/bar, where cP is the viscosity in centipoise.

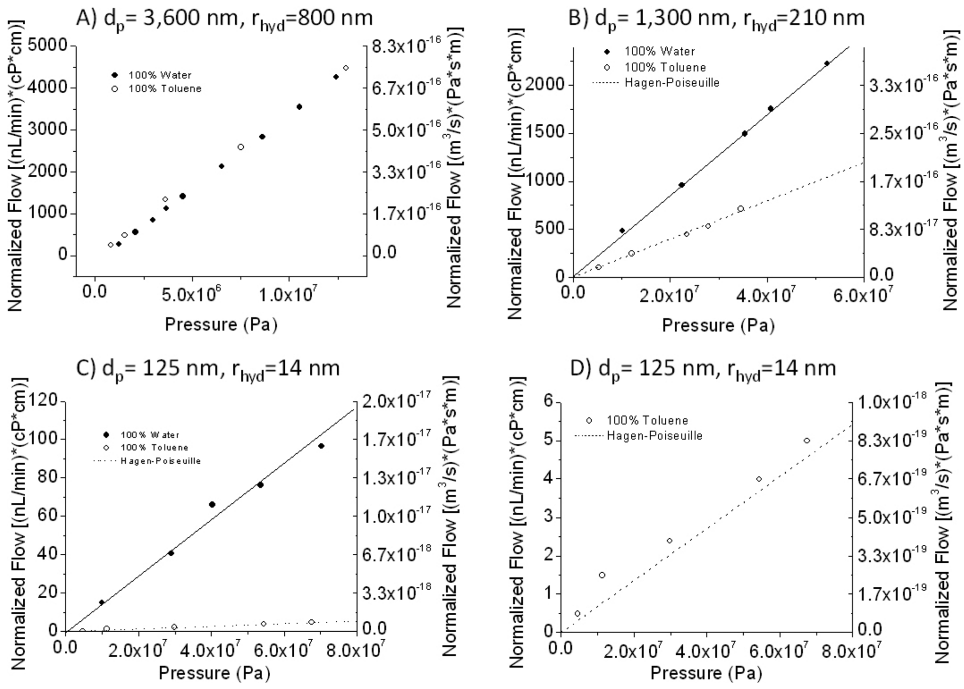

Figure 2. Pressure *vs* flow for 2 cm long capillaries packed with particles of varying diameter, where flow rate is normalized for viscosity and column length. (A) 3.6 μm diameter particles, (B) 1.3 μm diameter particles, (C) 125 nm particles, and (D) 125 nm particles displayed on expanded scale. Dashed line is calculated for Hagen–Poiseuille flow with no slip for each case where the porosity was determined independently. Solid lines are from least-squares fitting of the data. Flow rates are shown in common chromatographic units on the left axis and in MKS units on the right axis.

are the standard deviations of the slopes obtained from the linear regressions of pressure *vs* flow rate. The relative errors are propagated to obtain the errors for the flow enhancements listed in the table. For each particle size, the plots are linear and the toluene flow rate tracks the Kozeny–Carman behavior, whereas the water flow rate deviates by an amount that monotonically increases with decreasing particle diameter. One would expect no-slip flow for toluene, since its contact angle is 0° for this surface, and the agreement between the toluene and the slopes for the Kozeny–Carman equation is a check on the experimental accuracy.

Figure 3 shows a plot of flow enhancement *vs* hydraulic radius. The inset shows the plot on an expanded scale to include the 800 nm hydraulic radius, which exhibits negligible slip flow for water. The solid curve is a plot of eq 1, as determined by nonlinear regression, which fits well and reveals a slip length of 63 $\pm$ 3 nm. This slip length is within the wide range of the many earlier reports for water flow through carbonaceous channels. These are the first data, to our knowledge, for channels with low-energy surfaces and low contact angle, where the channel's radius is varied and multiple points are included below the slip length. In this case there are four data points for hydraulic radii below the slip length of 63 nm. The data are again low in noise due to the precision of the chromatographic instrument, providing a precise determination of the slip length.

Slip length has been reported to increase with shear rate for a flow measurement of water in a microchannel

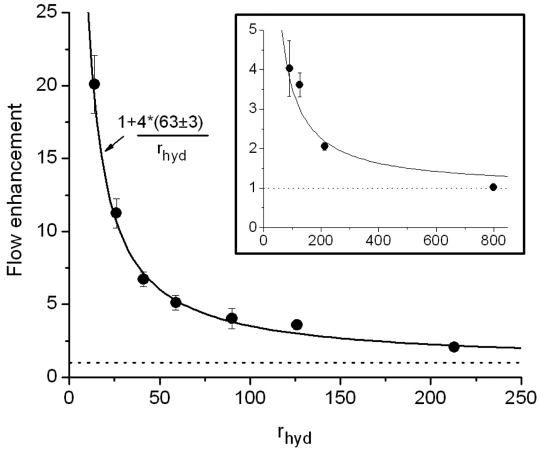

Figure 3. Flow rate enhancements for water compared to toluene are plotted *vs* hydraulic radius of the colloidal crystal. The error bars are standard deviations determined from the slopes for both water and toluene flow rates *vs* pressure. The curve is a nonlinear least-squares fit to eq 1, revealing L_s = 63 $\pm$ 3 nm. The dotted line indicates a flow enhancement of unity. The inset is the same plot on a different scale to include the data point for the hydraulic radius of 800 nm.

having a hydrocarbon surface.[12] Theory indicates that Newtonian fluids will exhibit non-Newtonian behavior at a sufficiently high shear rate that the fluid velocity exceeds the ability to equilibrate with the Lennard-Jones potential, leading to large increases in slip length.[32] The flow rates reported here easily accommodate the picosecond-scale Lennard-Jones equilibration. Theory also indicates that surface roughness is a

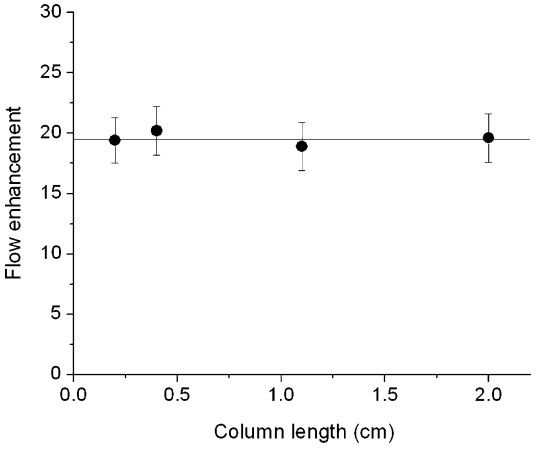

Figure 4. Plot of flow enhancement *vs* plug length for 125 nm particles, showing that flow enhancement is independent of shear rate for this range of experimental conditions.

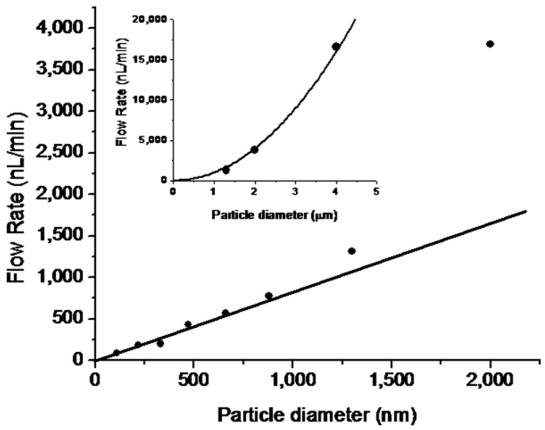

Figure 5. Dependence of flow rate on particle diameter with water as the fluid for a 1 cm plug length and a pressure of 1000 bar, showing a linear dependence for submicrometer particles. The solid line is a visual aid to see the points, and the solid curve is a parabola. Inset: Same plot, but now on the micrometer scale, showing a quadratic dependence on particle diameter in the no-slip limit.

factor contributing to a dependence of slip length on shear rate.[33] This is because an indentation filled with fluid would behave as a sticky surface in the limit of high shear rate. The possibility of a dependence of slip length on shear rate was investigated for the 15 nm hydraulic radius since surface roughness would affect its behavior the most. Fluid velocity was varied by reducing the length of the colloidal crystal, starting with the 2 cm length used for the flow enhancement study, and successively reducing the length down to 0.25 cm, which gives a 5-fold variation in fluid velocity. The results are shown in Figure 4, and these reveal no detectable shear rate dependence. To interpret whether this is reasonable, the contribution from surface roughness can be estimated. The colloidal silica used in this work was annealed the same way as commercial silica,[34] and annealed commercial silica is smooth on the subnanometer scale, with rare roughness features on the order of 2 nm in height and 20 nm in width.[35] The minimum time required for flow past a 20 nm feature at the maximum flow rate of 6 mm/s is 3 μs, whereas the time for exchange of water by self-diffusion[36] through the 2 nm height is 1 ns. It is concluded that it is reasonable for the slip length to have no shear rate dependence.

Slip flow is particularly interesting for chromatography, where zone variance scales with particle diameter. Commercial columns all use particles that exceed 1 μm in diameter, giving minimal slip flow, and smaller particles have been thought to be impractical since flow resistance scales with the inverse square of particle diameter. With slip flow, the flow resistance should no longer be quadratic in particle diameter. Figure 5 shows a plot of volume flow rate inside the medium as a function of particle size. The dependence on particle size is shown to be linear for particle diameters from 125 to 880 nm. The inset shows the quadratic dependence for particles above 1 μm in diameter. The flow rate is not normalized in this plot, thus showing how high the volume flow rate can be for packed 75 μm i.d. capillaries with a 1 cm bed length and a pressure of 1000 bar. The flow rate for the 125 nm particles is 87 nL/min, which is sufficient for electrospray mass spectrometry. The fluid velocity inside the medium is calculated to be 1.5 mm/s for the 75 μm i.d. capillary of 1 cm in length, which is reasonable for ultrahigh-performance liquid chromatography. These 125 nm particles are an order of magnitude smaller than those used in commercial chromatography, and to our knowledge, these are the first flow rate measurements for such small particle diameters.

CONCLUSIONS

A wetting liquid, toluene, exhibits Hagen–Poiseuille behavior in the no-slip limit for hydrocarbon-modified silica colloidal crystals with particles ranging in diameter from 125 nm to 4 μm. A nearly nonwetting liquid, water, exhibits slip flow through the same colloidal crystals for submicrometer particles. The data fit well to a slip length of 63 $\pm$ 3 nm. The slip length is independent of hydraulic radius and independent of shear rate, as expected for the spatial dimensions used in this work, in which the liquid is expected to exhibit continuum behavior. The results demonstrate the use of packed beds as a means of employing slip flow to gain high-volume flow rates.

MATERIALS AND METHODS

Silica colloids between 125 and 3600 nm were obtained from two sources (Nanogiant, Temple, AZ, and Fiber Optics, New Bedford, MA, USA) and were annealed by heating to 1050 °C for 3 h. The surfaces were fully rehydroxylated by refluxing the silica particles in 50:50 (v/v) HNO_3/H_2O for 3 h. A fused silica capillary

with a 75 μm i.d. was obtained from Polymicro (Phoenix, AZ, USA). The capillary was conditioned by pumping 0.1 M NaOH, 18 MΩ water, and ethanol with a syringe pump each for 30 min at 25 uL/min.

Colloidal crystals were packed into fused silica using methods described previously.[5] The surfaces were chemically modified by self-assembly of methyl and *n*-butyl trichlorosilanes (Gelest, Morrisville, PA, USA).[24] Columns were dried at 120 °C and stored in a desiccator prior to use.

Pressure−flow rate curves were generated with a Thermo Accela UHPLC (Thermo-Fisher Scientific, Waltham, MA, USA) with flow splitting provided by a microfluidic Tee (Vici Valco, Houston, TX, USA). The eluent was collected in a glass capillary sleeve with a 400 μm i.d. (Drummond Scientific Co., Broomall, PA, USA). The volume of eluent was determined by measuring the length of liquid that eluted into the sleeve with a Nikon SMZ 1500 Zoom microscope (Nikon, Tokyo, Japan). Both water and toluene measurements were taken with the HPLC grade solvents (Sigma Aldrich, St. Louis, MO, USA). Curve fitting was carried out with Origin software (Microcal, Northhampton, MA, USA).

Direct porosity measurements were taken with FRAP experiments. Briefly, columns were filled with sodium fluorescein (Sigma Aldrich) in 90:10 acetonitrile/water mixtures by wicking. The columns were immersed in oil and placed between glass coverslips on a Nikon Eclipse E2000 U inverted microscope. The dye was photobleached by a brief exposure to an argon ion laser (Melles Griot, Albuquerque, NM, USA), and the fluorescence recovery was monitored using a halogen light source (Nikon). A Cascade II CCD camera (Photometrics, Tuscon, AZ, USA) recorded all of the data. The recovery curves were compared to recovery curves generated in an open capillary, and the ratio of the recovery times was used as the porosity of the column.

Conflict of Interest: The authors declare the following competing financial interest(s): The senior author has a financial interest in a business that has licensed intellectual property for submicrometer silica particles applied to chromatography.

Acknowledgment. This work was supported by NIH under grant R01GM101464. The authors thank Scott Toth for his assistance in contact angle measurements and Sergey Suslov for assistance in obtaining SEM images.

Supporting Information Available: FRAP curves, plots of flow rate *vs* pressure, and SEM images for each particle diameter are provided. This material is available free of charge *via* the Internet at http://pubs.acs.org.

REFERENCES AND NOTES

1. Holt, J. K.; Park, H. G.; Wang, Y. M.; Stadermann, M.; Artyukhin, A. B.; Grigoropoulos, C. P.; Noy, A.; Bakajin, O. Fast Mass Transport through Sub-2-Nanometer Carbon Nanotubes. *Science* **2006**, *312*, 1034–1037.
2. Majumder, M.; Chopra, N.; Andrews, R.; Hinds, B. J. Nanoscale Hydrodynamics - Enhanced Flow in Carbon Nanotubes. *Nature* **2005**, *438*, 44–44.
3. Eijkel, J. C. T.; van den Berg, A. Nanofluidics: What Is It and What Can We Expect from It? *Microfluid. Nanofluid.* **2005**, *1*, 249–267.
4. Kalra, A.; Garde, S.; Hummer, G. Osmotic Water Transport through Carbon Nanotube Membranes. *Proc. Natl. Acad. Sci. U. S. A.* **2003**, 10175–10180.
5. Wei, B.; Rogers, B. J.; Wirth, M. J. Slip Flow in Colloidal Crystals for Ultraefficient Chromatography. *J. Am. Chem. Soc.* **2012**, *134*, 10780–10782.
6. Schure, M. R.; Maier, R. S.; Kroll, D. M.; Davis, H. T. Simulation of Ordered Packed Beds in Chromatography. *J. Chromatogr. A* **2004**, *1031*, 79–86.
7. Washburn, E. W. The Dynamics of Capillary Flow. *Phys. Rev.* **1921**, *17*, 273–283.
8. Thomas, J. A.; McGaughey, A. J. H. Reassessing Fast Water Transport through Carbon Nanotubes. *Nano Lett.* **2008**, *8*, 2788–2793.
9. Thomas, J. A.; McGaughey, A. J. H. Water Flow in Carbon Nanotubes: Transition to Subcontinuum Transport. *Phys. Rev. Lett.* **2009**, *102*.
10. Sinha, S.; Rossi, M. P.; Mattia, D.; Gogotsi, Y.; Bau, H. H. Induction and Measurement of Minute Flow Rates through Nanopipes. *Phys. Fluids* **2007**, *19*.
11. Whitby, M.; Cagnon, L.; Thanou, M.; Quirke, N. Enhanced Fluid Flow through Nanoscale Carbon Pipes. *Nano Lett.* **2008**, *8*, 2632–2637.
12. Choi, C. H.; Westin, K. J. A.; Breuer, K. S. Apparent Slip Flows in Hydrophilic and Hydrophobic Microchannels. *Phys. Fluids* **2003**, *15*, 2897–2902.
13. Cheng, J. T.; Giordano, N. Fluid Flow through Nanometer-Scale Channels. *Phys. Rev. E* **2002**, *65*.
14. Churaev, N. V.; Sobolev, V. D.; Somov, A. N. Slippage of Liquids over Lyophobic Solid-Surfaces. *J. Colloid Interface Sci.* **1984**, *97*, 574–581.
15. Huang, P.; Guasto, J. S.; Breuer, K. S. Direct Measurement of Slip Velocities Using Three-Dimensional Total Internal Reflection Velocimetry. *J. Fluid Mech.* **2006**, *566*, 447–464.
16. Tretheway, D. C.; Meinhart, C. D. Apparent Fluid Slip at Hydrophobic Microchannel Walls. *Phys. Fluids* **2002**, *14*, L9–L12.
17. Joseph, P.; Tabeling, P. Direct Measurement of the Apparent Slip Length. *Phys. Rev. E* **2005**, *71*.
18. Pit, R.; Hervet, H.; Leger, L. Direct Experimental Evidence of Slip in Hexadecane: Solid Interfaces. *Phys. Rev. Lett.* **2000**, *85*, 980–983.
19. Whitby, M.; Quirke, N. Fluid Flow in Carbon Nanotubes and Nanopipes. *Nat. Nanotechnol.* **2007**, *2*, 87–94.
20. Werder, T.; Walther, J. H.; Jaffe, R. L.; Halicioglu, T.; Koumoutsakos, P. On the Water-Carbon Interaction for Use in Molecular Dynamics Simulations of Graphite and Carbon Nanotubes. *J. Phys. Chem. B* **2003**, *107*, 1345–1352.
21. Mattia, D.; Calabro, F. Explaining High Flow Rate of Water in Carbon Nanotubes *via* Solid-Liquid Molecular Interactions. *Microfluid. Nanofluid.* **2012**, *13*, 125–130.
22. Mattia, D.; Gogotsi, Y. Review: Static and Dynamic Behavior of Liquids inside Carbon Nanotubes. *Microfluid. Nanofluid.* **2008**, *5*, 289–305.
23. Rafiee, J.; Mi, X.; Gullapalli, H.; Thomas, A. V.; Yavari, F.; Shi, Y. F.; Ajayan, P. M.; Koratkar, N. A. Wetting Transparency of Graphene. *Nat. Mater.* **2012**, *11*, 217–222.
24. Wirth, M. J.; Fairbank, R. W. P.; Fatunmbi, H. O. Mixed Self-Assembled Monolayers in Chemical Separations. *Science* **1997**, *275*, 44–47.
25. de Gennes, P.-G.; Brochard-Wyart, F.; Quere, D., *Capillarity and Wetting Phenomena: Drops, Bubbles, Pearls, Waves*; Springer: New York, NY, 2004.
26. Bird, R. B.; Stewart, W. E.; Lightfoot, E. N. *Transport Phenomena*; J. Wiley & Sons: New York, NY, 2007.
27. Rodbard, D.; Chrambach, A. Unified Theory for Gel Electrophoresis and Gel Filtration. *Proc. Natl. Acad. Sci.* **1970**, *65*, 970–977.
28. Giddings, J. C. *Unified Separation Science*; John Wiley & Sons, Inc.: New York, 1991.
29. Cabooter, D.; Billen, J.; Terryn, H.; Lynen, F.; Sandra, P.; Desmet, G. Detailed Characterisation of the Flow Resistance of Commercial Sub-2 μm Reversed-Phase Columns. *J. Chromatogr. A* **2008**, *1178*, 108–117.
30. Thompson, J. W.; Kaiser, T. J.; Jorgenson, J. W. Viscosity Measurements of Methanol-Water and Acetonitrile-Water Mixtures at Pressures up to 3500 bar Using a Novel Capillary Time-of-Flight Viscometer. *J. Chromatogr. A* **2006**, *1134*, 201–209.
31. Dymond, J. H.; Awan, M. A.; Glen, N. F.; Isdale, J. D. Transport Properties of Nonelectrolyte Liquid Mixtures. VIII. Viscosity Coefficients for Toluene and for Three Mixtures of Toluene + Hexane from 25 to 100°C at Pressures up to 500 MPa. *Int. J. Thermophys.* **1991**, *12*, 275–287.
32. Thompson, P. A.; Troian, S. M. A General Boundary Condition for Liquid Flow at Solid Surfaces. *Nature* **1997**, *389*, 360–362.
33. Niavarani, A.; Priezjev, N. V. Modeling the Combined Effect of Surface Roughness and Shear Rate on Slip Flow of Simple Fluids. *Phys. Rev. E* **2010**, *81*.
34. Newby, J. J.; Legg, M. A.; Rogers, B.; Wirth, M. J. Annealing of Silica to Reduce the Concentration of Isolated Silanols and Peak Tailing in Reverse Phase Liquid Chromatography. *J. Chromatogr. A* **2011**, *1218*, 5131–5135.

35. Legg, M. A.; Wirth, M. J. Probing Topography and Tailing for Commercial Stationary Phases Using AFM, FTIR, and HPLC. *Anal. Chem.* **2006**, *78*, 6457–6464.
36. Holz, M.; Heil, S. R.; Sacco, A. Temperature-Dependent Self-Diffusion Coefficients of Water and Six Selected Molecular Liquids for Calibration in Accurate H-1 NMR PFG Measurements. *Phys. Chem. Chem. Phys.* **2000**, *2*, 4740–4742.